The mechanism of failure of wood in bending

The Mechanism of Failure of Wood in Bending

Sur le mécanisme de rupture du bois en flexion

Das Bruchverhalten des Baustoffes Holz unter Biegungsbeanspruchung

JOHANNES MOE
Dr. techn., Norwegian Institute of Wood Working and Wood Technology,
Blindern, Norway

1. Introduction

The basic mechanism of failure of wood in bending has been discussed by a number of investigators. References are made to contributions by BAUMANN [1], BEGHTEL and NORRIS [2], COMBEN [3], NEWLIN and TRAYER [4], NORÉN [5] and YLINEN [6].

During an experimental investigation conducted by the author in order to study strength and stiffness of laminated timber beams, a study was also undertaken on the mechanism of failure. The experimental investigation was not very well suited for such a study of the basic properties of wood in bending, since the beams were produced from materials which contained the natural growth characteristics such as knots and other strength reducing factors.

It is hoped, however, that some of the observations and the theoretical derivations described below may contribute somewhat toward a better understanding of the problem under consideration.

2. Symbols

A	timber of highest structural grade (T 390)
B	timber of medium structural grade (T 300)
C	timber of lowest structural grade (T 210)
D	timber not passing as structural material
A_0	cross sectional area

L length of specimen
b width of beam
c distance between wrinkles
d deformation of axially loaded specimen
d_0 deformation of axially loaded specimen at maximum load
h height of beam
αh distance from the neutral axis to the tensile face of the beam
βh distance from the neutral axis to the root of the wrinkle
γh depth of the wrinkle
l_1 length over which beam deflections were measured
y measured deflections
Δ deformation in a wrinkle
ρ radius of curvature
P applied load
P_w applied load at the formation of the first wrinkle
P_{max} ultimate load
M, M_w, M_{max} corresponding values of applied bending moment
σ_w bending stress at the formation of the first wrinkle
σ'_T compressive strength parallel to grain
σ_s tensile strength
ϵ_0 compressive strain at the formation of a wrinkle
ϵ_1 average strain on the compressive face of a beam
p ratio σ_s/σ_w
n factor accounting for the average reduction in compressive strength after the formation of wrinkles
k factor accounting for the variation in strain between the wrinkles
Φ form factor

3. Experimental Investigation

Fourtyseven laminated timber beams with the nominal dimensions of $7 \times 20 \times 450$ cm were loaded to destruction as indicated in Fig. 1. The span/depth-ratio was so large that the effect of the shear force on the mode of failure was insignificant [2]. The beams were divided into three series (0.1 and 2) with lamination thicknesses of 16, 22 and 45 mm, respectively.

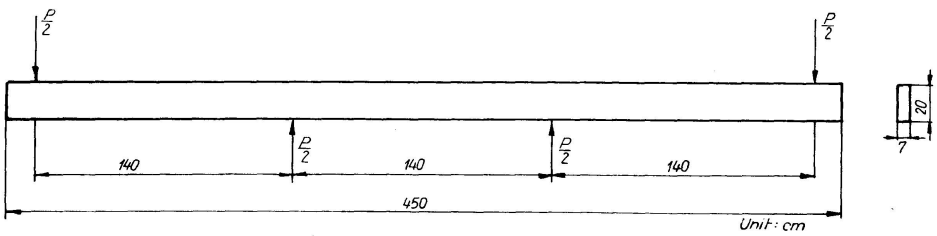

Fig. 1. Nominal Dimensions of Beams.

Table I. Test Results — Series 0

Beam No.	Measured			Ratio	σ_w	σ'_T	Ratio	Estimated	Computed		
	P_w	P_{max}	γ	P_{max}/P_w			σ_w/σ'_T	y_{max}[1])	Δ[2])	n	σ_s
	kg	kg			kg/cm²	kg/cm²		mm	mm		kg/cm²
0 AB 1	3930	4570	0.305	1.160	540	463	1.165	10	1.3	0.601	830
4	4050	4130	0.148	1.022	551	429	1.284	8.5	0.5	0.522	650
5	4150	4325	0.178	1.042	540	544	0.993	11	0.8	0.535	665
6	3900	4350	0.300	1.115	506	527	0.961	10.5	1.4	0.562	750
0 CD 1	3430	3920	0.404	1.142	463	547	0.848	11	1.9	0.542	800
2	3000	3820	0.304	1.272	404	469	0.863	12.0	1.5	0.700	650
3	3040	3900	0.280	1.282	412	576	0.716	6.5	0.7	0.732	640
4	3150	3610	0.205	1.145	428	656	0.652	10	0.9	0.658	575

Table II. Test Results — Series 1

Beam No.	Measured			Ratio	σ_w	σ'_T	Ratio	Estimated	Computed		
	P_w	P_{max}	γ	P_{max}/P_w			σ_w/σ'_T	y_{max}[1])	Δ[2])	n	σ_s
	kg	kg			kg/cm²	kg/cm²		mm	mm		kg/cm²
1 AB 1	4600	4975	0.450	1.082	670	555	1.205	15	2.5	0.487	1205
2	3400	3465	0.115	1.018	496	435	1.140	7	0.3	0.523	566
3	3275	4260	0.379	1.297	486	488	0.994	14	2.0	0.660	880
6	3300[1])	4160	0.400	1.260	494	>447	<1.105	17	2.6	0.625	905
1 AD 1	3000	3920	0.453	1.306	451	522	0.865	15	2.6	0.625	920
2	3600[1])	3950	0.333	1.097	544	497	1.094	11	1.4	0.536	835
3	4200	4660	0.443	1.108	620	662	0.937	16	2.7	0.507	1120
4	3600	4020	0.219	1.117	534	670	0.798	11	0.9	0.610	720
5	3630[1])	4250	0.229	1.171	535	558	0.960	12	1.0	0.666	750
1 BC 1	3600	4250	0.400	1.181	536	497	1.080	17	2.6	0.570	940
2	3700	4200	0.405	1.135	567	>477	<1.187	16	2.5	0.535	980
3	2700	3340	0.291	1.237	444	415	1.070	12	1.3	0.680	695
5	3400	4030	0.373	1.182	500	574	0.872	11	1.6	0.584	850
1 BD 1	3000	3750	0.213	1.250	442	560	0.787	10.5	0.8	0.782	630
2	3500	3960	0.298	1.130	514	594	0.865	8.5	1.0	0.576	770
1 CD 1	3400[1])	4055	0.200	1.193	500	635	0.787	12	0.9	0.728	680
2	3200[1])	3370	0.125	1.053	472	520	0.907	9	0.4	0.588	550
3	2700[1])	3265	0.175	1.207	396	414	0.957	9	0.6	0.786	530
4	3700	4360	0.360	1.176	552	512	1.078	13	1.8	0.585	915
5	3100	3520	0.432	1.135	460	547	0.842	9	1.4	0.528	820
B 1	3100[1])	4275	0.347	1.380	456	598	0.762	13	1.7	0.750	820

[1]) Estimated from deflection curves.
[2]) Computed from formula (16) with $c = 2h$.

Table III. Test Results — Series 2

Beam No.	Measured			Ratio	σ_w	σ'_T	Ratio	Estimated	Computed		
	P_w	P_{max}	γ	P_{max}/P_w			σ_w/σ'_T	y_{max}[1])	Δ[2])	n	σ_s
	kg	kg			kg/cm²	kg/cm²		mm	mm		kg/cm²
2 BC 1	2650	3640	0.430	1.373	399	516	0.773	17	2.3	0.683	810
2	2350	3220	0.444	1.368	355	453	0.783	16.0	2.7	0.670	735
3	2850	3720	0.455	1.303	428	529	0.812	12.5	2.1	0.626	875
4	3300	3530	0.221	1.070	498	692	0.722	9.5	0.8	0.553	655
5	3300	3350	0.177	1.013	502	525	0.955	8.5	0.6	0.495	600
2 CD 1	2530	3110	0.312	1.230	382	618	0.617	10	1.2	0.657	610
2	2500	3420	0.328	1.368	376	535	0.716	11	1.4	0.762	655
3	2900	3670	0.443	1.264	443	622	0.713	12	2.0	0.602	870
4	2750	3510	0.333	1.275	417	573	0.727	12	1.5	0.679	700
5	2500	3650	0.464	1.461	379	561	0.676	12.5	2.2	0.716	850
2 E 1	2850	3520	0.262	1.235	430	470	0.914	11.5	1.1	0.704	645
2	2850	3910	0.288	1.372	432	643	0.682	12	1.3	0.807	715

[1]) Estimated from the deflection curves.
[2]) Computed from formula (16) with $c = 2h$.

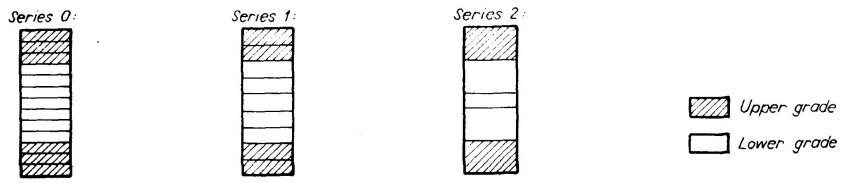

Fig. 2. Cross-Sections of the Beams.

The structural grading of the timber was carried out in accordance with the Norwegian Standard 447 [7], and each beam was produced from two different grades, as indicated in Fig. 2 and Tables I, II and III. The beams are designated according to the grade combinations in such a manner that beam no 1-AB-2 is, for instance, the second companion specimen belonging to series 1 which is produced from grades A and B (see Notations).

A picture of the loading system is shown in Fig. 3. A number of electrical strain gages of 8 or 20 mm gage lengths were attached to most of the beams of series 1. A comparison between the measured deflections and the strains indicated that the strain gages throughout the tests showed 15 to 20 percent lower strains than the true values. There is, however, no reason to believe that the recorded distribution of strains is significantly wrong.

Some of the test results, which relate to the theoretical study of the present paper, are presented in Tables I, II and III. A more detailed report on the experimental investigation is published in Norsk Skogindustri [8].

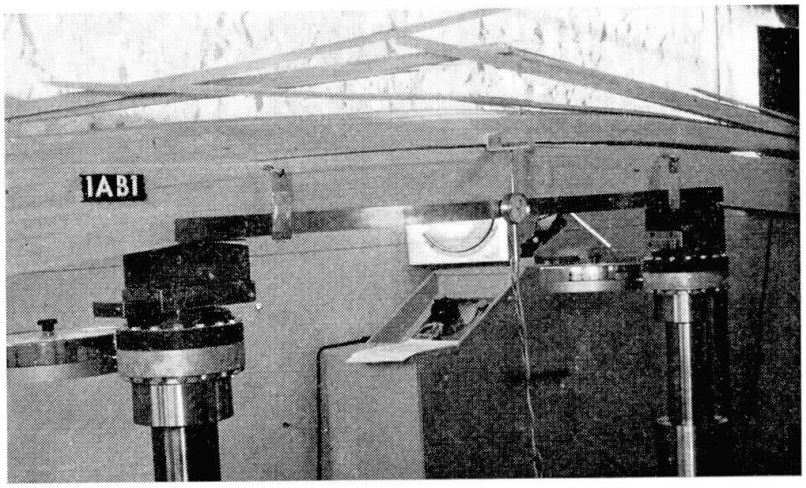

Fig. 3. Test Arrangement.

4. Strains and Stresses

Typical diagrams of the observed distribution of strains across the depth of a beam at its center are shown in Fig. 4. The variation in strains at increasing load is shown in Fig. 5.

For practical purposes it can be said that the strains varied rectilinearly across the depth as long as there was no sign of failure in the compression zone of the beam.

At a load which in the authors tests ranged between 70 and 100 percent of the ultimate, there appeared a number of wrinkles in the region which had the highest compressive stresses. These wrinkles often started out from knots,

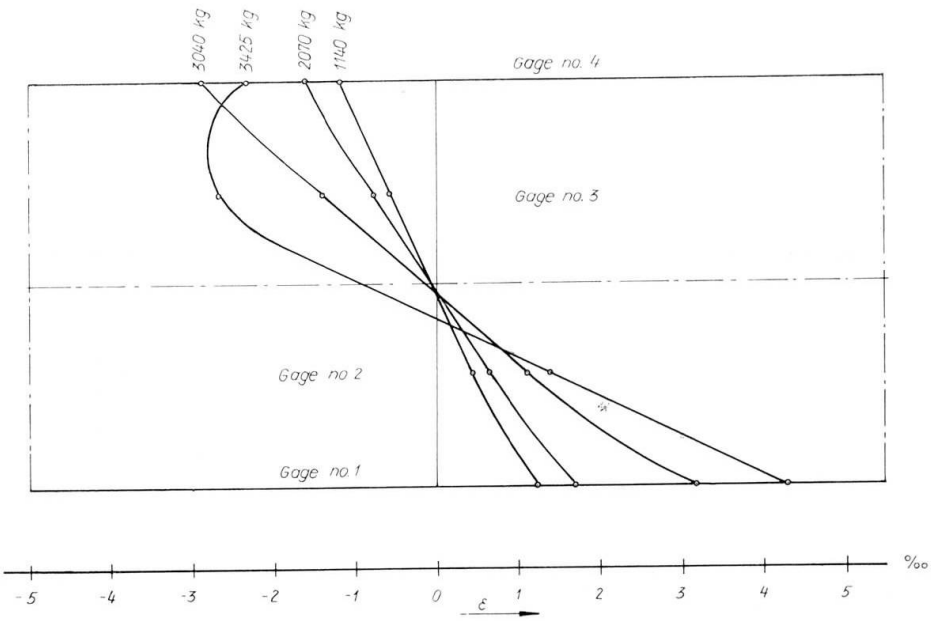

Fig. 4. Strains at Mid-Section of Beam No. 1 AD 1,

and developed gradually further into the compression zone. Fig. 6 shows three beams where the wrinkles have been inked in order to show up on the photograph.

When the load exceeded that which caused the formation of such wrinkles (P_w), the strains in the gages on the compression side of the beam dropped. The strains in the gages on the tension side and in those close to the neutral axis on the compression side now increased at an increasing rate, as Fig. 5 indicates. At the same time the neutral axis moved toward the tension side. None of the gages represented by Figs. 4 and 5 were intersected by the wrinkles.

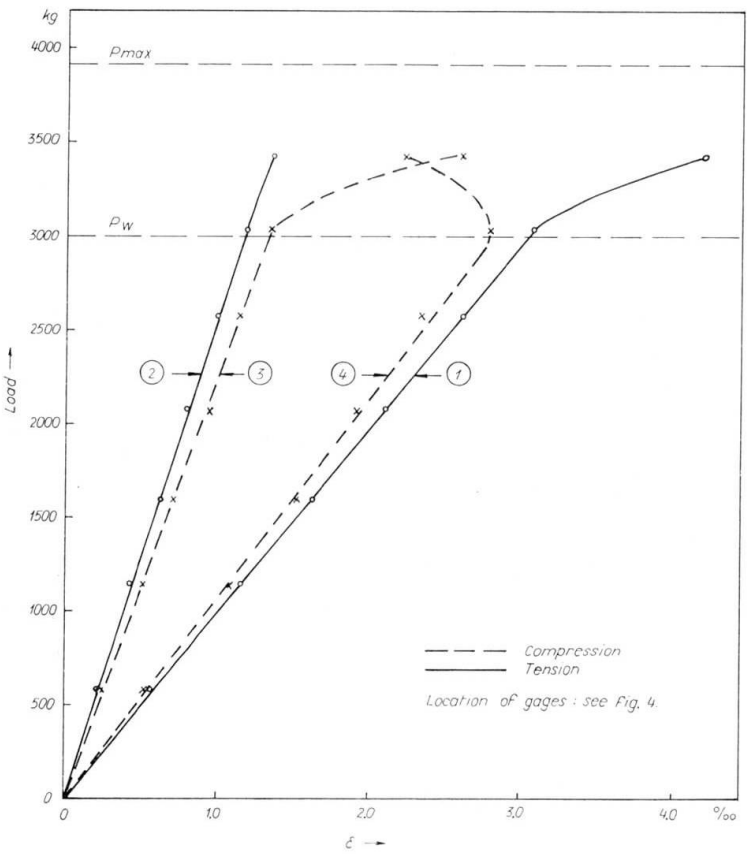

Fig. 5. Strains at Mid-Section of Beam No. 1 AD 1.

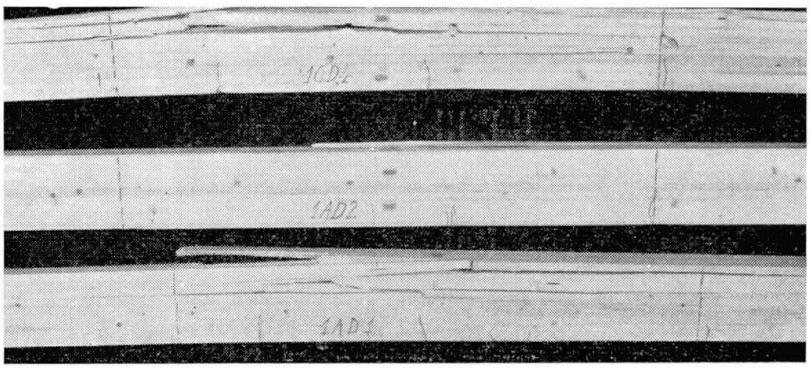

Fig. 6. Beams Loaded to Failure.

The stresses in a beam may be computed by means of the conventional bending theory as long as $P \leqq P_w$. The bending stresses (σ_w) in the extreme fibres of the tested beams at the formation of the first wrinkles are listed in Tables I, II and III. Only the beams in which wrinkles developed are included in the tables. Local wrinkles at the points of load application were disregarded. The clear wood compressive strength (σ'_T) of the outer lamination on the compression side of each beam is also presented in the tables. Fig. 7 shows that σ_w is on the average slightly lower than σ'_T, which is to be expected on account of the knots in the beams. COMBEN [3] states that the wrinkles in his tests started to develop at a load approximately equal to the compressive strength of the wood. NEWLIN and TRAYER [4] on the contrary base their theory on the assumption that the compressive strength of wood in bending is higher than that in uniaxial compression.

As soon as the wrinkles have appeared, the stress distribution is completely changed. The stresses on the compression face of the beam do not increase beyond σ_w at increasing load. The increasing deformations are from now on confined to the wrinkles, where the strains increase rapidly. Due to these large strains, the strength of this zone soon starts to drop.

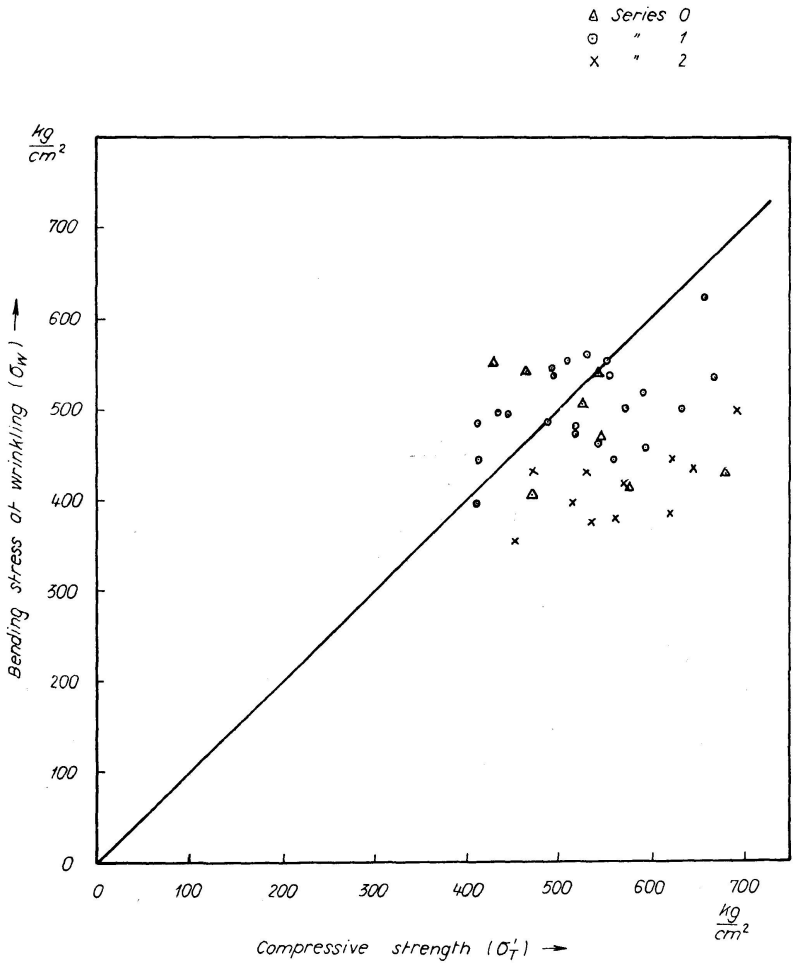

Fig. 7. Comparison of σ_w with σ'_T.

A qualitative picture of the stress distribution across the height of the beam after the formation of the wrinkles is shown in Fig. 8. The depth of the beam may after the appearance of the wrinkles be divided into the following three zones, counted from the tension side:

1. The zone of elastic tensile stresses (height: αh).
2. The zone of elastic compressive stresses (height: βh).
3. The zone of wrinkling (height: γh).

In the third zone the wood between the wrinkles is in the elastic stage, and the strains are here slightly lower than those causing new wrinkles to appear.

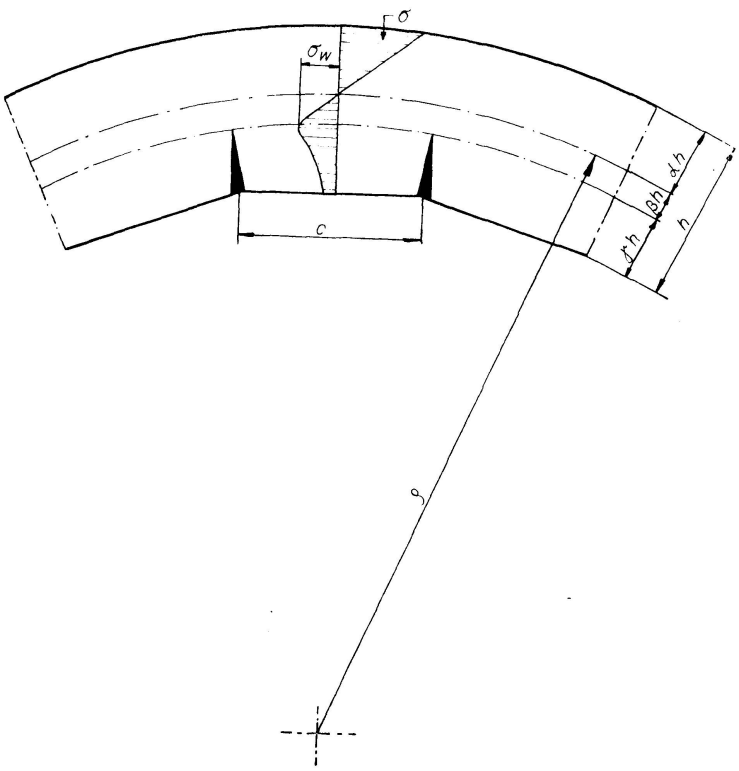

Fig. 8. Schematic Picture of Beam with Wrinkles.

Specimens loaded in axial compression parallel to the grain direction behave analogously. The strains are in this case uniform along the length of the specimen up to the maximum load, at which the wrinkles appear. By a continued application of load after the maximum value has been passed, the load drops and all the deformations are from now on concentrated in the wrinkles. Fig. 9 shows load-deformation relationship obtained in this manner.

Returning now to Fig. 8, the average compressive strain (ϵ_1) along the lower face of the beam may be derived from the following equation:

$$\frac{\epsilon_1}{\epsilon_0} = \frac{(\beta+\gamma)h}{\beta h} = 1+\frac{\gamma}{\beta}, \tag{1}$$

where ϵ_0 is the strain in wood at which formation of wrinkles occur, i. e. the strain at a distance of γh from the compression side of the beam.

The amount of deformation (Δ) which has to be absorbed in one wrinkle may be estimated from the formula

$$\Delta = (\epsilon_1 - k\,\epsilon_0)\,c = \left(1 - k + \frac{\gamma}{\beta}\right)\epsilon_0\,c\,, \tag{2}$$

where c is the distance between the wrinkles,
k is a factor that accounts for the decrease in the strain between the wrinkles after their formation.

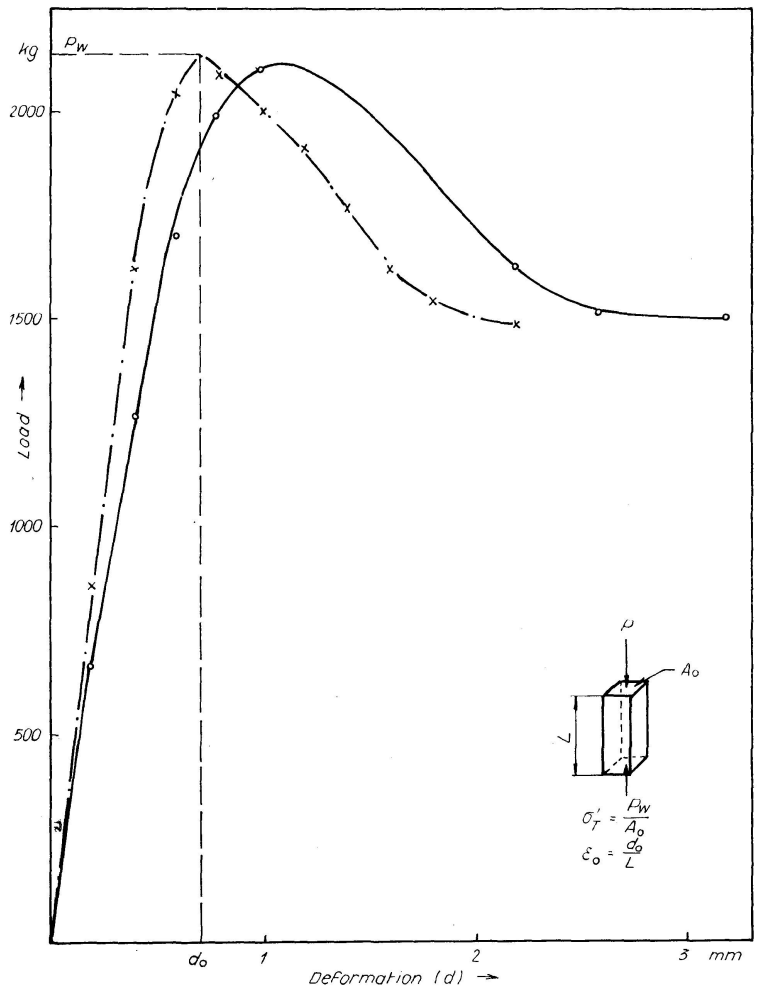

Fig. 9. Load-Deformation-Curves in Axial Compression.

5. Ultimate Strengths

The author believes that a stress distribution such as that indicated by the dotted curve of Fig. 10 should be introduced in the expression for the ultimate strength. The author's tests did not, however, yield sufficient information

about the form of this curve, which should be determined on the basis of numerous diagrams such as those presented in Fig. 9.

The reduced strength of the compression zone, following the formation of the wrinkles can, however, be demonstrated through an analysis based on the simplified stress distribution shown with full lines in Fig. 10. This analysis will be presented below and the results will be compared with test results.

It is assumed that the moduli of elasticity are equal in tension and compression. This is not always true. However, tests by the author as well as others [3] showed that the position of the neutral axis at low loads was close to the middle height of the beams, which indicates that the difference between the two moduli is small.

The quantities α, β and γ in Fig. 10 may be determined by means of the following equations, which apply to a beam with no axial load:

$$\sigma_s/\sigma_w = \alpha/\beta = p, \tag{3}$$

$$\alpha+\beta+\gamma = 1, \tag{4}$$

$$^1/_2\,\alpha h\,\sigma_s = {}^1/_2\,\beta h\,\sigma_w + \gamma h n\,\sigma_w. \tag{5}$$

Choosing γ as the independent variable and solving for p, β and α, one obtains:

$$p = \frac{1-\gamma+2n\gamma}{1-\gamma}, \tag{6}$$

$$\beta = \frac{(1-\gamma)^2}{2(1-\gamma+n\gamma)}, \tag{7}$$

$$\alpha = \frac{(1-\gamma)(1-\gamma+2n\gamma)}{2(1-\gamma+n\gamma)}. \tag{8}$$

The variations of α, β and p with γ are shown in Fig. 11 for a value of n equal to 2/3.

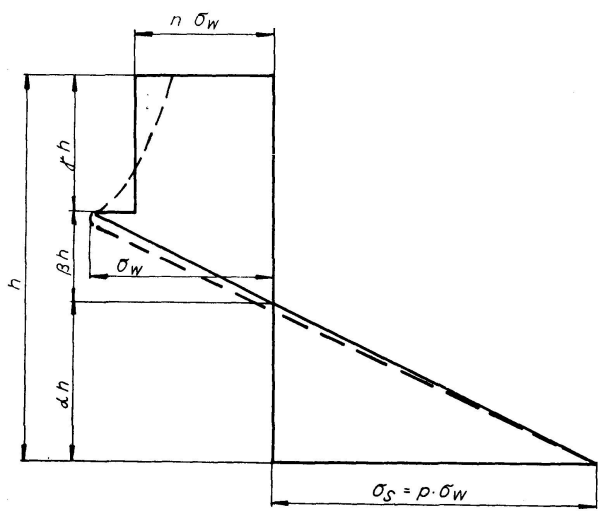

Fig. 10. Assumed Stress Distribution at Ultimate Load.

The moment capacity of the stress condition shown in Fig. 10 is computed by the formula

$$M = \frac{b}{2}\sigma_s \alpha h^2\left(1-\frac{\alpha}{3}\right) - \frac{b}{2}\sigma_w \beta h^2\left(\gamma+\frac{\beta}{3}\right) - n\gamma b h^2 \sigma_w \frac{\gamma}{2},$$

which, by introduction of expressions (7) and (8), yields:

$$M = \Phi \frac{1}{6}\sigma_w b h^2, \tag{9}$$

where

$$\Phi = n(4-\gamma)\gamma + (1-\gamma)^2. \tag{10}$$

The bending moment at which the wrinkles start to develop is found from formulas (9) and (10) by introducing $\gamma = 0$, which yields $\Phi = 1$. Hence

$$M_w = \frac{1}{6}\sigma_w b h^2. \tag{11}$$

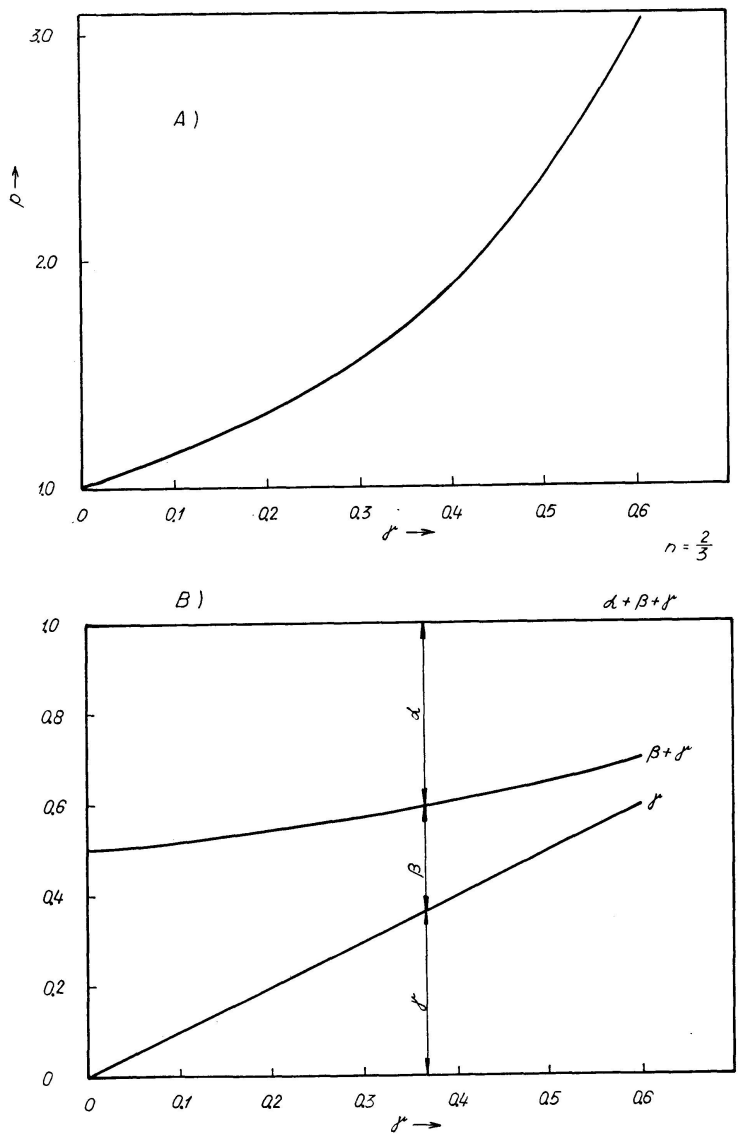

Fig. 11. Relationships Betweem α, β, γ and p.

Introduction of Eq. (11) in (9) yields

$$M = \Phi M_w. \tag{12}$$

The ratios of $\Phi = M/M_w = P/P_w$

at failure, as observed from the author's tests, are listed in Tables I, II and III and shown graphically in Fig. 12 as a function of the measured value of γ. Fig. 12 also shows curves representing the computed values of Φ for different values of n. Fig. 12 clearly indicates that the increase in strength after the first formation of wrinkles is comparatively small, and that it is justified to assume a drop in the strength of the compression zone due to the formation of the wrinkles.

The factor n and the tensile strength σ_s may be computed by the introduction of the observed values of Φ and γ into Eqs. (10), (3) and (6). The computed values of n and σ_s are listed in Tables I, II and III. There is a slight tendency for the computed tensile strength to be on the average highest for the materials

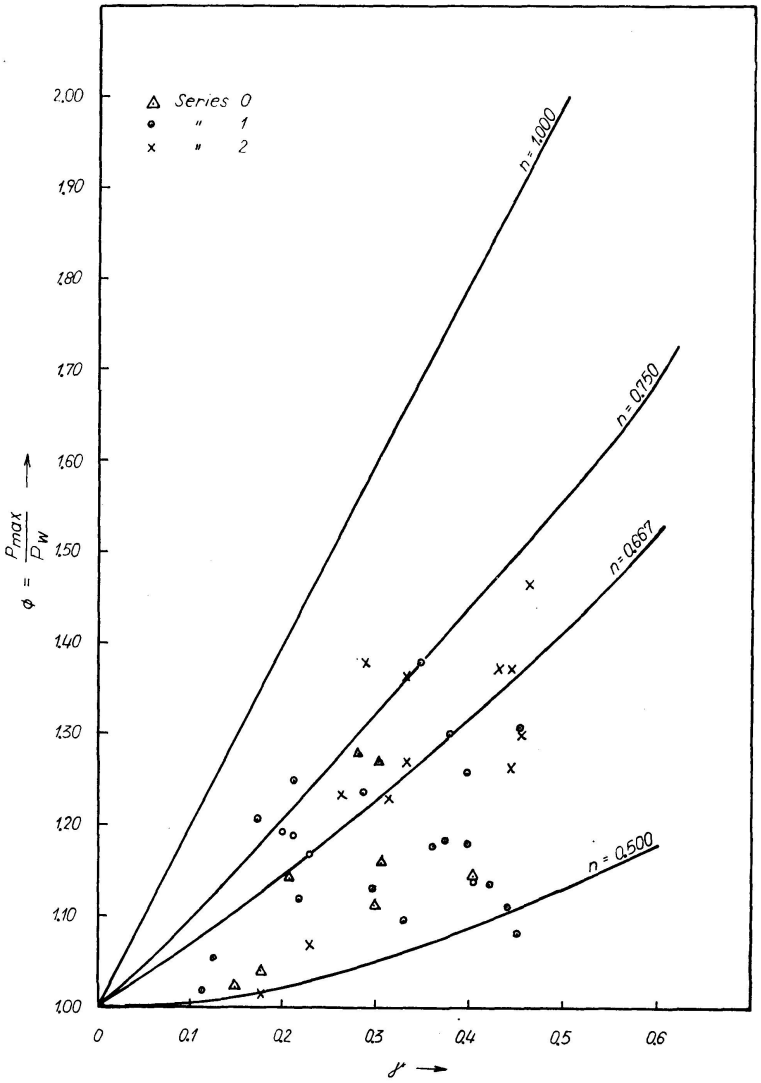

Fig. 12. Comparison of Observed and Calculated Relationship Between ϕ and γ.

of the highest structural grades, as should be expected. The values of n range between 0.485 and 0.807.

The scatter in the test results is large. This scatter is partly due to the assumed simplified stress distribution, which does not satisfactorily express the behaviour of wood. Besides, the fact that the wrinkles developed through several laminations with varying compressive strength, and the presence of knots in the laminations, also contribute to the large scatter.

6. Deformations in the Wrinkles

If the coefficient k in Eq. (2) is assumed equal to unity, one obtains the following expression for the deformation in one of the wrinkles:

$$\Delta = \gamma c \frac{\epsilon_0}{\beta}. \tag{13}$$

Referring to Fig. 8, the radius of curvature (ρ) of the deflected beam is given by the expression.

$$\frac{1}{\rho} = \frac{\epsilon_0}{\beta h}, \tag{14}$$

where ϵ_0 is the strain at the root of the wrinkle.

The average radius of curvature may be computed from the observed deflection (y) measured over a length (l_1) with constant bending moment by the following formula

$$\rho = \frac{l_1^2}{8y}. \tag{15}$$

Introduction of Eqs. (14) and (15) into Eq. (13) finally yields

$$\Delta = \frac{8\gamma c h y}{l_1^2}. \tag{16}$$

In order to be able to compute Δ from Eq. (16) it is necessary to know the distance (c) between the wrinkles. Fig. 6 shows the positions of the wrinkles in some of the beams tested by the author. It was, for the purpose of demonstration, assumed that $c = 2h$ and Δ was then computed for all the tested beams on the basis of the measured values of y and γ. A comparison of the computed values of Δ (see Tables I, II and III) with Fig. 9 shows that they are certainly sufficiently large to cause a pronounced drop in the strength of the wood.

7. Effect of Height on the Bending Strength

It is a well known fact that the bending strength (modulus of rupture) of timber beams depends upon the height of the beam. Fig. 13 shows the effect of height as determined from a number of beams tested by COMBEN [2].

It will be shown below that it is possible to find what seems to be a reasonable explanation of the height effect by means of the theory developed in the present paper. This explanation is based upon the stress diagram which is shown with the dotted curve of Fig. 10.

From Eq. (16) it is apparent that the amount of deformation in a wrinkle is proportional to the distance c between the wrinkles. Fig. 9 shows, furthermore, that the strength of wood decreases as the deformation in the wrinkle increases.

It will now be postulated that the distance between the wrinkles increases with increasing height of the beam. If this is true, then the strength of a large specimen, measured by means of the conventional bending stresses, will be lower than that of a smaller one, on account of the larger deformations in the wrinkles.

It seems quite reasonable to assume that c is a function of h, as indicated above. The stress gradient across the depth of a high beam is smaller than

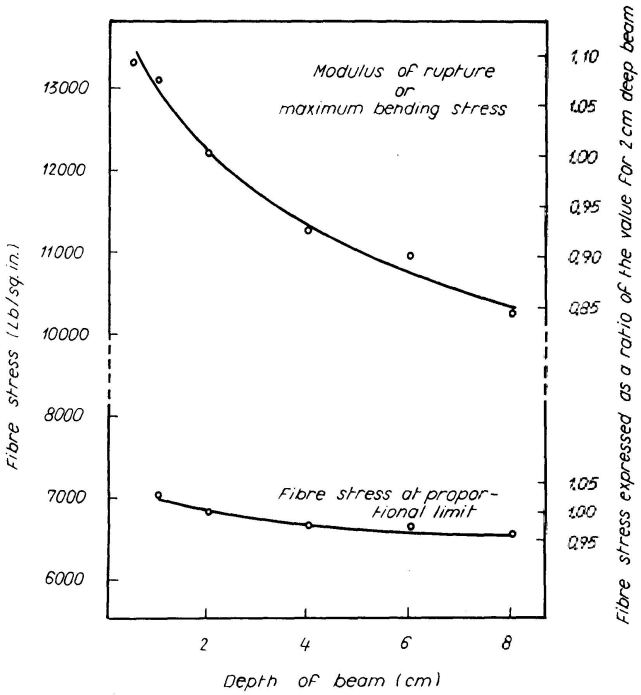

Fig. 13. Relationship Between Fibre Stress and Depth of Beam.

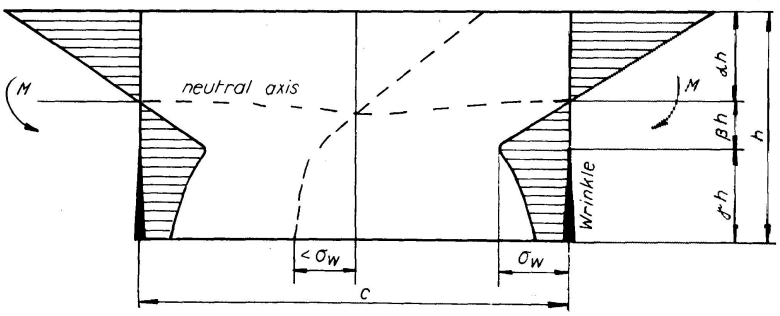

Fig. 14. Free-Body Diagram of the Beam portion Between Two Adjacent Wrinkles.

that of a shallow one. When the first wrinkle developes, it is therefore likely that it immediately penetrates deeper into the high beam than into the shallow one.

The situation after the formation of the first wrinkle is schematically illustrated in Fig. 14. The portion of the beam between two neighbouring wrinkles may be treated as a free body to which the stresses indicated across the end sections are applied. These stresses are equivalent to a couple at each end.

If the material were elastic, homogeneous and isotropic, the principle of Saint-Venant would postulate that, within a certain distance from the end sections, the stresses would vary linearly across the entire depth of the section. The deviations from this latter distribution at the end sections may be considered as local edge disturbances. The distance to the point where the effects of such disturbances are negligible depends upon the height of the beam.

Due to the low shear modulus of wood parallel to its direction of grains, the dampening of the edge disturbances will be slower than in an isotropic material. The distance between the wrinkles is governed by the condition that the dampening should not be so large that the stresses between the wrinkles at any point exceed the compressive strength of the wood.

The dampening described above will cause a change in the position of the neutral axis, as indicated in Fig. 14.

8. Conclusions

The theory which has been presented on the preceding pages may yield an explanation to the mechanism of failure of wood in bending. Experimental verification is, however, necessary. Tests should be carried out on clear wood beams of varying dimensions, during which close attention should be devoted to the development of the wrinkles as well as the deformations and the strains in the region of constant bending moment.

Analytical investigations of the distribution of stresses in the body between two neighbouring wrinkles will also lead to a better understanding of the mechanism of failure. The anisotropic character of the wood should, of course, be considered in such studies.

9. Acknowledgement

This study was undertaken on the basis of observations made during an experimental investigation carried out as a cooperative research project between the Norwegian Building Research Institute and the Norwegian Institute of Wood Working and Wood Technology. The project was sponsored by the Royal Norwegian Council for Scientific and Industrial Research.

10. References

1. Baumann, R.: Die bisherigen Ergebnisse der Holzprüfung in der Materialprüfungsanstalt an der Techn. Hochschule Stuttgart. Forsch. Ing.-Wes. H. 231, Berlin 1922.
2. Beghtel S. C., and Norris C. B.: "Strength of Wood Beams of Rectangular Cross Section as Affected by Span-Depth Ratio." Forest Products Laboratory, Madison, Report No. R 1910, 1952.
3. Comben, A. J.: "The Effect of Depth on the Strength Properties of Timber Beams." Dept. of Scientific and Industrial Research, Forest Products Research, Special Report No. 12, London 1957.
4. Newlin, J. A., and Trayer, G. W.: "Form Factors of Beams Subjected to Transverse Loading Only." Forest Products Laboratory, Madison, Report No. 1310, 1941.
5. Norén, Bengt: «Limmade träbalkars böjhållfasthet.» Teknisk Tidsskrift, Vol. 87, No. 38, pp. 903—908, 1957.
6. Ylinen, Arvo: «Über den Einfluß der Probekörpergröße auf die Biegefestigkeit des Holzes.» Holz als Roh- und Werkstoff, Vol. 5, No. 9, pp. 299—305, 1942.
7. Norsk Standard 447, Norges Standardiserings-Forbund, Oslo, 1958, 11 pp.
8. Moe, Johannes: "Strength and Stiffness of Glued Laminated Timber Beams." Norsk Skogindustri Vol. 15, No. 5, pp. 189—199, 1961 (in English).

Summary

A theory of the basic mechanism of failure of wood in bending is outlined which qualitatively accounts for the well known height effect on the strength of timber beams. The theory agrees in certain important respects with experimental findings obtained through tests of more than forty laminated timber beams. Further experimental verification is necessary.

Résumé

L'auteur esquisse une théorie sur le mécanisme fondamental de rupture du bois en flexion, théorie qui permet d'expliquer qualitativement l'influence bien connue de la hauteur d'une poutre en bois sur sa résistance. Sous certains rapports importants, la théorie est confirmée par les résultats d'essais effectués sur plus de quarante poutres collées. Cette vérification expérimentale doit cependant être poursuivie.

Zusammenfassung

Der Autor skizziert eine Theorie über das Bruchverhalten von auf Biegung beanspruchten Holzträgern. Diese Theorie erlaubt es ihm, eine qualitative Erklärung des wohlbekannten Einflusses der Balkenhöhe auf die Festigkeit des Holzträgers zu geben. In gewissen wichtigen Punkten zeigt sie eine gute Übereinstimmung mit den an vierzig und mehr verleimten Holzträgern ermittelten Versuchsergebnissen. Trotzdem werden weitere Versuche zur Bestätigung dieser Theorie notwendig sein.